Check for updates

Estimates of quantal synaptic parameters in light of more complex vesicle pool models

Simone Brachtendorf[†], Grit Bornschein[†] and Hartmut Schmidt*

Carl Ludwig Institute of Physiology, Medical Faculty, Leipzig University, Leipzig, Germany

The subdivision of synaptic vesicles (SVs) into discrete pools is a central concept of synaptic physiology. To better explain specific properties of transmission and plasticity, it was initially suggested that the readily releasable pool (RRP) of SVs is subdivided into two parallel pools that differ in their release probability. More recently, evidence was provided that sequential pools with a single RRP and a series-connected finite-size replenishment pool (RP) inserted between the reserve pool (RSP) and RRP equally well or even better account for most aspects of transmission and plasticity. It was further suggested that a fraction of the presynaptic release sites (N) are initially unoccupied by SVs, with vesicle replenishment occurring rapidly during activity. Furthermore, the number of release sites itself changes with rapid dynamics during activity. Experimentally, it is difficult to obtain insights into the organization of SV pools directly and the interpretation of the data typically requires complex modeling. In this study, we propose a framework that identifies specific signs of the presence of the series-connected RP without complex modeling, using a combination of two experimental electrophysiological standard methods, cumulative analysis (CumAna) and multiple probability fluctuation analysis (MPFA). CumAna uses cumulative EPSC amplitude plots recorded during trains of action potentials and estimates the pool of releasable SVs from the y-intercept (y(0)) of a linear fit to the amplitudes late in the train. MPFA estimates N (N_{MPFA}) from a parabolic fit to a variance−mean plot of EPCS amplitudes recorded under conditions of different release probabilities. We show here, in particular, that if $y(0) > N_{MPFA}$ this is a strong indication for a series-connected RP. This is due to the fact that y(0) reports the sum of RRP and RP. Our analysis further suggests that this result is not affected by unoccupied release sites as such empty sites contribute to both estimates, y(0) and N_{MPFA}. We discuss experimental findings and models in the recent literature in light of our theoretical considerations.

KEYWORDS

pool models, cumulative analysis, quantal parameters, MPFA method, replenishment

Introduction

The concept of Ca^{2+}-dependent quantal vesicular release was introduced to synaptic physiology in the 1950s by Bernhard Katz et al. based on electrophysiological findings (Fatt and Katz, 1952; Del Castillo and Katz, 1954). The idea of quantal transmitter release received further support by the invention of rapid-freezing combined with timed synaptic stimulation and electron microscopy. Heuser and Reese succeeded in catching synaptic vesicles (SVs) in the act of fusion (Heuser et al., 1979). The concept of quantal release has since been confirmed in several studies and further extended (Neher, 2015). In this view, the amplitude of a postsynaptic current (PSC) is given by PSC = $p\,n\,q$, where p is the average probability that a vesicle (or "unit" as it was called initially) fuses, n is the number of fusion-competent SVs and q the amplitude of the postsynaptic response resulting from the fusion of a single vesicle. The

latter is referred to as the "quantal size" and the product of p and n is referred to as the "quantal content (QC)." Hence, the amplitude of a PSC is the product of quantal content and quantal size and the overall rate of synaptic failures (F) or successes (S) strictly depends on the quantal parameters, being given by $F = (1-p)^n$ and $S = 1 - F$.

The total number of fusion-competent vesicles constitutes the readily releasable pool (RRP) of SVs. Fusion occurs at specific presynaptic release sites (N) or docking sites as a synonym. However, quantitative estimates of RRP and N frequently deviate from each other and their relationship is not fully clear (Neher, 2015). The relationship between RRP and N and the reasons underlying discrepancies between estimates of RRP and N are one of the topics of this article.

During synaptic activity, the RRP needs to be replenished by a continuous supply of SVs in order to maintain synaptic function. This supply comes from additional SV pools that have been postulated in recent years (Neher, 2015). SVs run through different Ca^{2+}-dependent and Ca^{2+}-independent steps that include docking and priming to become fully fusion-competent SVs of the RRP (Neher and Brose, 2018; Silva et al., 2021). Furthermore, the size of the RRP or the N can change during activity, which according to recent findings is a major determinant of synaptic short-term plasticity (reviewed, e.g., in Neher and Brose, 2018; Miki, 2019; Schmidt, 2019; Neher, 2023). Models with sequential pools of SVs have been proposed that accounted for several experimental findings on transmitter release and short-term plasticity at different synapses in the cerebellum (Miki et al., 2016; Doussau et al., 2017), the neocortex (Bornschein et al., 2019b), the brainstem (Lin et al., 2022), and the hippocampus (Aldahabi et al., 2024).

We will distinguish three types of sequential models here. In the first type, presynaptic release sites are at rest fully occupied by SVs forming the RRP. During synaptic activity, the RRP gets replenished from SVs that occupy replenishment sites and form a replenishment pool (RP) with a finite size that is intermediate between the reserve pool (RSP) and the RRP. While we use "replenishment" throughout the manuscript, there are other frequently used synonyms including "replacement" or "recruitment." The number of release sites itself can increase during high-frequency activity, thereby giving rise to synaptic facilitation (Doussau et al., 2017). We refer to this model as the sequential occupied sites (SOS) model (Figure 1A). The second type

is similar to the first type, but at rest, part of the release sites are considered to be not occupied by SVs. During high-frequency activity, the occupancy but not the number of release sites increases, thereby again accounting for synaptic facilitation (Miki et al., 2016). While this model has been referred to as the replacement site/docking site model previously, we refer to it as the sequential empty sites model here for clarity (SES; Figure 1B). The third model also has a fixed number of release sites and includes empty sites. In this model, SVs are first in a loosely docked and primed state (LS) and reversibly pass through a tightly docked and primed state (TS) prior to fusion. An increase in TS accounts for facilitation here. This model is referred to as the LS/TS model (Figure 1C) (Neher and Brose, 2018; Neher, 2023). While SVs in the TS correspond to the RRP in the narrower sense, SVs in the LS are not identical to the RP vesicles (see Discussion).

Therefore, in order to account for short-term plasticity, in these sequential models, either it is assumed that the occupancy of a fixed number of N is incomplete at rest and increases during activity, i.e., the RRP increases but not the N (SES and LS/TS) (Trigo et al., 2012; Miki et al., 2016; Neher and Brose, 2018; Neher, 2023), or it is assumed that the number of N itself (= RRP) increases (SOS) (Valera et al., 2012; Brachtendorf et al., 2015; Doussau et al., 2017). Both phenomena are sometimes referred to as 'overfilling'. In all models, the increase in the size of the RRP is viewed as activity-dependent and reversibly. In any case, the result is paired-pulse facilitation (PPF) as observed, e.g., at cerebellar parallel-fiber (PF) synapses. The results obtained with rapid-freezing electron microscopy methods showed a reversible increase in the number of docked SVs shortly after timed synaptic stimulation (Kusick et al., 2020; Kusick et al., 2022), which is consistent with the sequential models and reversible overfilling. However, it does not differentiate between the three types of models.

An alternative and earlier model proposes a subdivision of the RRP into two parallel pools, differing in their vesicular release probabilities (p_v) (Wölfel et al., 2007; Hallermann et al., 2010; Mahfooz et al., 2016). In traditional parallel models, the intermediate RP is not implemented (Wölfel et al., 2007; Mahfooz et al., 2016). We refer to the traditional parallel model as the PP model here (Figure 1D). In a recent study, it was found that sequential and parallel models may almost equally well describe different aspects of experimental data (Eshra et al., 2021; Weichard et al., 2023). Therefore, it is difficult to distinguish not only
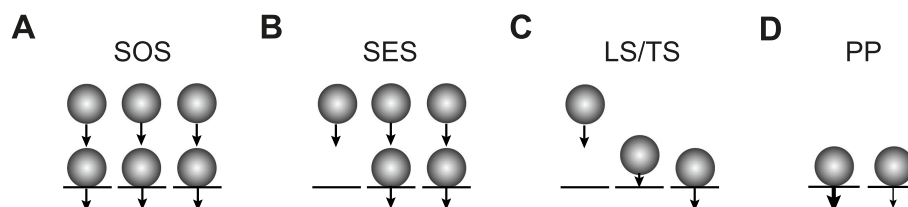

FIGURE 1
Three types of sequential pool models and a parallel pool model. **(A)** In the SOS model, all release sites (N, black lines) are occupied by SVs (spheres) at rest, forming the RRP (lower row). Release probability p_v is homogenous across sites as indicated by the identical arrows. In addition, there are replenishment sites that are occupied by SVs forming the RP (upper row). The reserve pool is omitted for clarity. During high-frequency synaptic activity, N reversibly increases, thereby giving rise to facilitation (Doussau et al., 2017). **(B)** In the SES model, not all N are occupied at rest. During high-frequency synaptic activity, the occupancy of N but not the number of N itself reversibly increases, thereby giving rise to facilitation (Miki et al., 2016). **(C)** In the LS/TS model, SVs reversibly shift between loosely (LS, middle) and tightly docked states (TS, right). There are also empty sites as in **(B)** (left). Fusion occurs only from the TS state. The LS/TS ratio is influenced by synaptic activity and determines short-term plasticity (Neher and Brose, 2018). Note that LS vesicles are attached to a release site while RP vesicles occupy replacement sites. Therefore, LS and RP vesicles are not identical. **(D)** In the PP model, the RRP is subdivided into two parallel pools with different vesicular release probabilities (different arrows). Replenishment occurs directly from the reserve pool without an intermediate RP (Wölfel et al., 2007; Mahfooz et al., 2016).

between the different sequential models but also between the sequential and parallel models.

Two standard electrophysiological methods are frequently used for the quantitative estimation of synaptic parameters, including SV pools: the analysis of cumulative PSC amplitude plots (CumAna) (Schneggenburger et al., 1999) and variance–mean analysis or multiple probability fluctuation analysis (MPFA) as a synonym (Clements and Silver, 2000). In CumAna, trains of action potentials (APs) are applied under recording conditions suitable to drive synapses into equilibrium between release and replenishment. This is typically given if the vesicular release probability (p_v) is sufficiently high to achieve a steady-state depression of ~60% during the train. At synapses with moderate p_v, this may require performing recordings in an elevated extracellular Ca^{2+} concentration ($[Ca^{2+}]_e$). Additional methodological requirements for the successful application of CumAna have been described in detail elsewhere (Neher, 2015). The result is a linear relationship between cumulative PSC amplitudes late in the train and the corresponding stimulus numbers or times. Fitting a line to this linear phase and extrapolating it to the y-intercept removes the contribution of SVs added via replenishment in the steady-state phase. Hence, the y-intercept is thought to report the initial size of the RRP. More precisely, it reports a value close to the decrement of the RRP during the train and the "real" size of the RRP can be obtained with a correction calculation as long as the RRP gets strongly depleted during the train (Thanawala and Regehr, 2013; Neher, 2015). Dividing the first PSC or quantal content by the y-intercept then gives the average p_v.

For MPFA, PSCs are recorded under conditions of several different p-values, which are typically obtained by changing the $[Ca^{2+}]_e$. Alternative approaches to change p include broadening the presynaptic AP, e.g., by application of blockers of voltage-gated potassium channels such as TEA or 4-AP. The variance and the mean of the PSCs are calculated during stable recording periods after the wash-in of each different Ca^{2+} solution or alternative treatment and the variance is plotted against the mean. A parabolic fit to these data yields N and the average release probability per release site (p_N) (Clements and Silver, 2000).

In our experiments at cortical synapses, we typically found that the estimates of RRP from the y-intercept were larger than the estimates of N from MPFA for the same synapses. Accordingly, the estimates of the p-values showed the opposite behavior (Schmidt et al., 2013; Baur et al., 2015; Bornschein et al., 2019a; Bornschein et al., 2019b). Deviations between y-intercept and N were observed also at many other synapses (Table 1) (Neher, 2015). However, the cause of these deviations is not fully clear.

CumAna and MPFA were established before the development of sequential or parallel pool models. Here, we used computer simulations to systematically investigate which entities are actually reported by the two experimental methods in light of different pool models and considering incompletely populated release sites. The systematic approach starts with basic simulations of simple arrangements of SV pools, which become increasingly complex. This article aimed to investigate how much information about the organization of SVs can be obtained based on the experimental results alone, without the need to fit complex models to the data. We suggest that a combination of CumAna with MPFA provides complementary insights into the functional organization of SV pools and their dynamics that cannot be achieved with either method alone.

Methods

Computer simulations

All simulations were performed in Mathematica 14 (Wolfram) as described in more detail elsewhere (Wender et al., 2023).

Algebraic simulations

For the algebraic simulations of CumAna with the SOS and PP models, it was assumed that the vesicular release probability p_v remains constant during a train of APs. The number of APs during a train was chosen to ensure the effective steady-state required for CumAna. In the absence of replenishment, 20 to 25 APs were used. With replenishment, 100 APs were used in all cases, but trains are shown truncated for clarity. The number of release sites occupied by a releasable vesicle ($n[i]$) during the ith pulse of a train was calculated as follows:

$$n[i] = n[i-1] - p_v * n[i-1] + r \qquad (1)$$

where $p_v * n[i-1]$ is the release in the preceding pulse and r is the replenishment rate per stimulus from the RSP. The quantal content of the ith pulse is given by $n[i] * p_v$. In simulations mimicking the presence of a series-connected RP, the RP was simulated as follows:

$$n1[i] = n1[i-1] - r_1 * n1[i-1] + r_2 \qquad (2a)$$

TABLE 1 Experimental results obtained for y(0) and N for various model synapses.

Synapse	y(0)	N	Model
Calyx of Held	~1,500 (Lin et al., 2022)	~600 (Meyer et al., 2001)	LS/TS (Lin et al., 2022)
PF–PC	~10 (Valera et al., 2012; Wender et al., 2023)	~3 (Schmidt et al., 2013)	SOS (Doussau et al., 2017)
PF–MLI	~8* (Silva et al., 2024)	~4 (Malagon et al., 2016; Silva et al., 2024)	SES (Miki et al., 2016)
L5PN–L5PN	~20 (P8-10) ~28 (P21-24) (Bornschein et al., 2019a)	~8 (age independent) (Bornschein et al., 2019b)	SOS (Bornschein et al., 2019a)

This table is not meant to provide a full review of existing data. We do apologize to all colleges whose important work is not referenced here.
*Calculated from the normalized values given in Silva et al. (2024).
PF, parallel fiber; PC, Purkinje cell; MLI, molecular layer interneuron; L5PN, layer 5 pyramidal neuron.

and the RRP by

$$n[i] = n[i-1] - p_v * n[i-1] + r_1 * n1[i] \qquad (2b)$$

Two parallel pools were simulated using Equation 1 for each RRP and the $n[i]$ from the two pools were summed linearly, assuming independence of release sites.

In the presence of replenishment, the y-intercept ($y(0)$) underestimates the size of the RRP but can be corrected, using the following formula (Neher, 2015):

$$y(0)_{corr} = \frac{y(0) - QC_n}{1 - \dfrac{QC_n}{QC_1}} \qquad (3)$$

where QC are the quantal contents during the last (n) or first stimulation, respectively. An alternative correction (Thanawala and Regehr, 2013) assumes a restricted number of release sites, while our simulations allowed for variability in the N or their occupancy according to recent models of short-term plasticity (Miki et al., 2016; Doussau et al., 2017; Bornschein et al., 2019b; Lin et al., 2022; Aldahabi et al., 2024). Hence, the alternative correction was not considered further here.

Stochastic simulations

For Monte Carlo simulations of release for CumAna (SES model) and MPFA (all release models), random real numbers were generated for p_v or p_N, respectively, and p_{occ} and p_{repl} using 'RandomReal' of Mathematica and compared to the corresponding set values. Release from a given release site occurred only if the conditions set for p_v or p_N and p_{occ} were met by the corresponding random numbers. If a release site had already been released, release from this same site could occur again, only if the conditions of p_v or p_N and p_{repl} were met by the corresponding random numbers. Release sites were simulated individually, and the total response was obtained by assuming that quantal contents were added linearly across the release sites.

For fitting the variance–mean plots of MPFA, the binominal model with the following parabolic function was used:

$$\sigma^2 = \overline{QC} - \frac{\overline{QC}^2}{N} \qquad (4)$$

where σ^2 is the variance and $\overline{QC}$ the mean of the quantal content. As in our simulations, QC lacks components of EPSC fluctuations, such as variations in q or heterogeneous p_v, that contribute to σ^2 in experiments, different from real MPFA (Silver, 2003), the simple binominal parabola could be used here.

Results

Basic simulations of CumAna and MPFA

For CumAna, we started with a simple algebraic simulation of a single RRP set to 10 SVs with p_v set to 0.6 in the absence of any replenishment (Figure 2A). All release sites were assumed to be fully

occupied; i.e., the RRP corresponded to N in these simulations. The value of 10 was chosen as the rounded value that reflects, for example, the number of release sites at neocortical pyramidal neuron synapses (Bornschein et al., 2019b). Simulations throughout the manuscript were also performed for N of 3 representative, e.g., of cerebellar parallel-fiber synapses (Valera et al., 2012; Schmidt et al., 2013). The principal results and conclusions were identical for both settings of N and, therefore, for clarity only the simulations for the value of 10 are presented in the following.

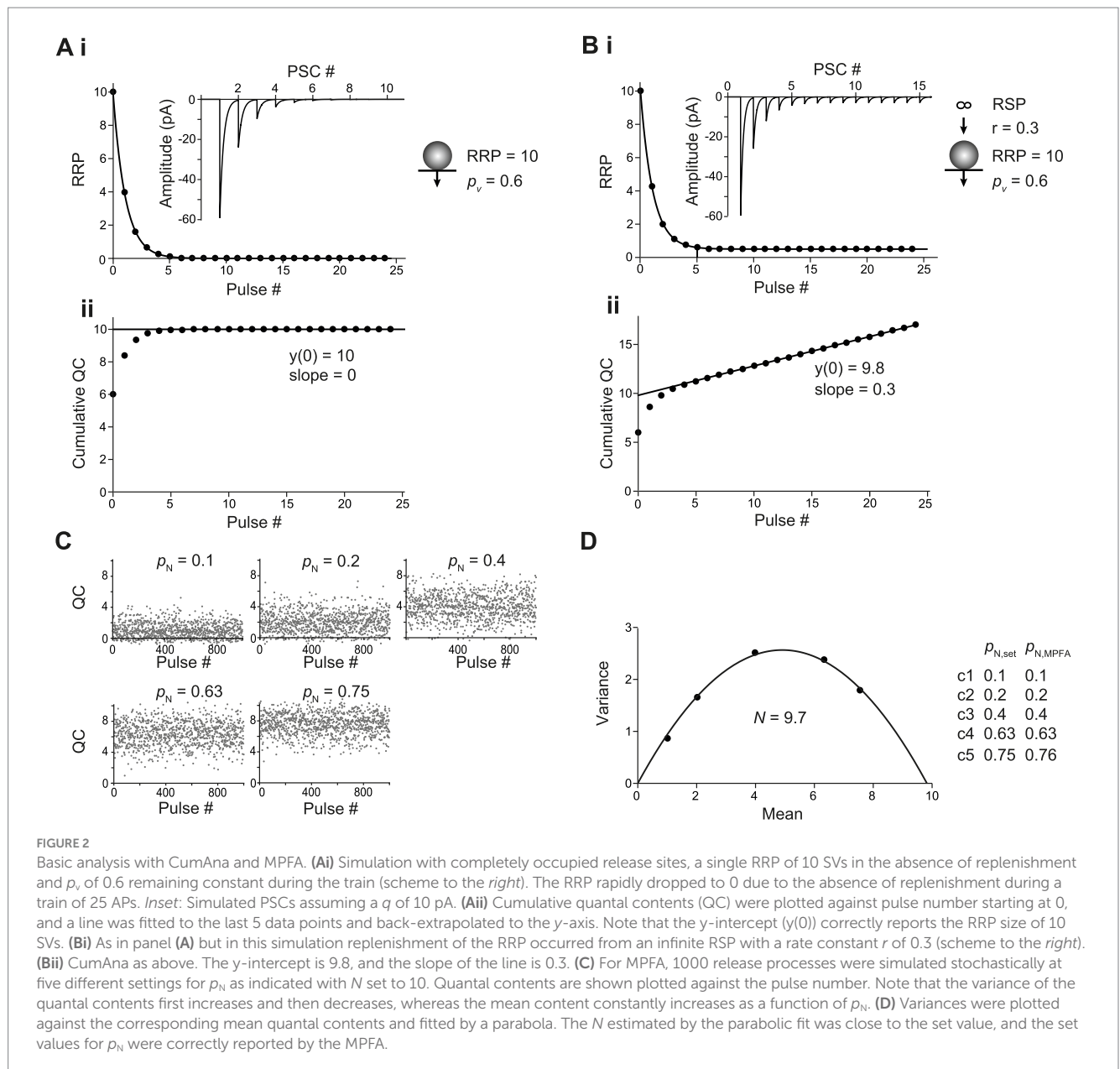During a train of APs, the RRP was rapidly exhausted, giving rise to a horizontal line fit in the CumAna plot. In this most simple scenario, the y-intercept correctly reports the RRP size of 10, and dividing the first QC by the y-intercept (QC1/$y(0)$) gives the set value of p_v of 0.6. Hence, in this very simple scenario the nominal values and the actual values reported by CumAna perfectly match. The slope of the line is zero, according to the absence of replenishment.

Next, the simulation was extended to include replenishment with a constant rate r of 0.3 per stimulus from an infinite RSP (Equations 2a,b; Figure 2B). In this scenario, the slope of the line fit reported the r of 0.3. However, the y-intercept currently slightly underestimated the size of the RRP, being 9.8 rather than 10. Accordingly, p_v was slightly overestimated. For this scenario, the y-intercept can be corrected by analytical calculations (Equation 3 in Methods) to yield the set value of the RRP of 10 and to derive the correct p_v of 0.6 (Neher, 2015).

For MPFA, we started with stochastic simulations of 10 fully occupied N with homogenous release probability (p_N), which were assumed to be fully replenished between pulses (Figure 2C). The p_N was set to different values such that the parabola was well defined, i.e., the larger p_N exceeded 0.5, which is the apex of the parabola that has to be passed for a reliable fit (Clements and Silver, 2000). The parabolic fit (Equation 4) resulted in an N_{MPFA} of ~10, which is the intercept of the parabola with the x-axis. Depending on the number of simulated release processes, the x-axis intercept fluctuated more or less strongly around the set value of 10. Even with the 1,000 runs used in these simulations, which cannot be achieved experimentally, the deviation from the set value was up to 0.3 (Figures 2C,D). The deviation from the set value was reduced to 0.01 after 10,000 runs. The p_N obtained from the parabolic fits reliably reported the set values even with 1,000 runs. In summary, in these basic scenarios, both CumAna and MPFA provide reliable estimates of the "real values" for RRP, number of release sites, and p-values that are congruent between the two analysis methods.

CumAna in SOS and PP model

To investigate CumAna for the SOS model, we inserted the finite-sized RP between RSP and RRP in the simulation (Figure 3). As above, all release sites were assumed to be fully occupied initially (Doussau et al., 2017). The p_v of SVs in the RRP was set to 0.6 as above. The sum of SVs in RP and RRP was set to 10. The transition of SVs from the infinite RSP to the finite RP occurred with rate constant r_2. The transition of SVs from RP to RRP occurred with a faster rate constant r_1. r_1 was either only moderately faster than r_2, which resulted in immediate depression (Figure 3A), or it was much faster than r_2, leading to overfilling of the RRP during the first APs and initial facilitation despite the high p_v (Figure 3B). These models thus simulate experimental results and their interpretation, where a key determinant

FIGURE 2
Basic analysis with CumAna and MPFA. **(Ai)** Simulation with completely occupied release sites, a single RRP of 10 SVs in the absence of replenishment and p_v of 0.6 remaining constant during the train (scheme to the *right*). The RRP rapidly dropped to 0 due to the absence of replenishment during a train of 25 APs. *Inset*: Simulated PSCs assuming a q of 10 pA. **(Aii)** Cumulative quantal contents (QC) were plotted against pulse number starting at 0, and a line was fitted to the last 5 data points and back-extrapolated to the y-axis. Note that the y-intercept (y(0)) correctly reports the RRP size of 10 SVs. **(Bi)** As in panel **(A)** but in this simulation replenishment of the RRP occurred from an infinite RSP with a rate constant r of 0.3 (scheme to the *right*). **(Bii)** CumAna as above. The y-intercept is 9.8, and the slope of the line is 0.3. **(C)** For MPFA, 1000 release processes were simulated stochastically at five different settings for p_N as indicated with N set to 10. Quantal contents are shown plotted against the pulse number. Note that the variance of the quantal contents first increases and then decreases, whereas the mean content constantly increases as a function of p_N. **(D)** Variances were plotted against the corresponding mean quantal contents and fitted by a parabola. The N estimated by the parabolic fit was close to the set value, and the set values for p_N were correctly reported by the MPFA.

of short-term plasticity is the transition rate of SVs from a series-connected RP to the RRP (Miki et al., 2016; Doussau et al., 2017; Schmidt, 2019). It should be noted that in experiments, next to overfilling, mechanisms that increase p_v during trains may contribute to facilitation. Therefore, for studying changes in pool size, it is recommended to aim at keeping p_v constant, e.g., by adjusting the $[Ca^{2+}]_e$ (Neher, 2015). We also ran CumAna simulations with increasing p_v during the train (data not shown), which did not affect the following conclusions regarding the y-intercept in CumAna reports and its relationship to MPFA. The p_v reported will be the initial p_v at the beginning of the train rather than the facilitated p_v late in the train.

In the simulations with RP and RRP, and constant p_v and r values, the curve of the decrease in QC was biphasic (Figure 2Ai,Bi) due to the presence of the finite-sized RP. RRP will show the same behavior, but scaled by p_v. This is a clear deviation from the monophasic

decrease in QC observed in the simulations in which the RRP was directly replenished from the RSP (Figure 2). A biexponential decay can thus indicate the presence of a finite-sized RP (Bornschein et al., 2019a), but it could also indicate a subdivision of the RRP into two parallel pools (see paragraph after next).

We found that the fitting line of the corresponding CumAna plots had a slope of r_2. The slope was independent of r_1 and solely determined by the rate-limiting transition rate r_2. Remarkably, the y-intercept did not correspond to the size of the RRP but had a value close to 10. Thus, the y-intercept actually reflects a value close to the sum of RP and RRP. Accordingly, the p_v value calculated from the ratio of QC1 or PSC1 to the y-intercept significantly underestimated the specified value of 0.6 (Figure 3Aii,Bii).

For CumAna with the PP model, the RRP was subdivided into two subpools with different p_v and replenishment rates (Wölfel et al., 2007; Mahfooz et al., 2016). RRP1 harbored 3 SVs with a high p_{v1} of
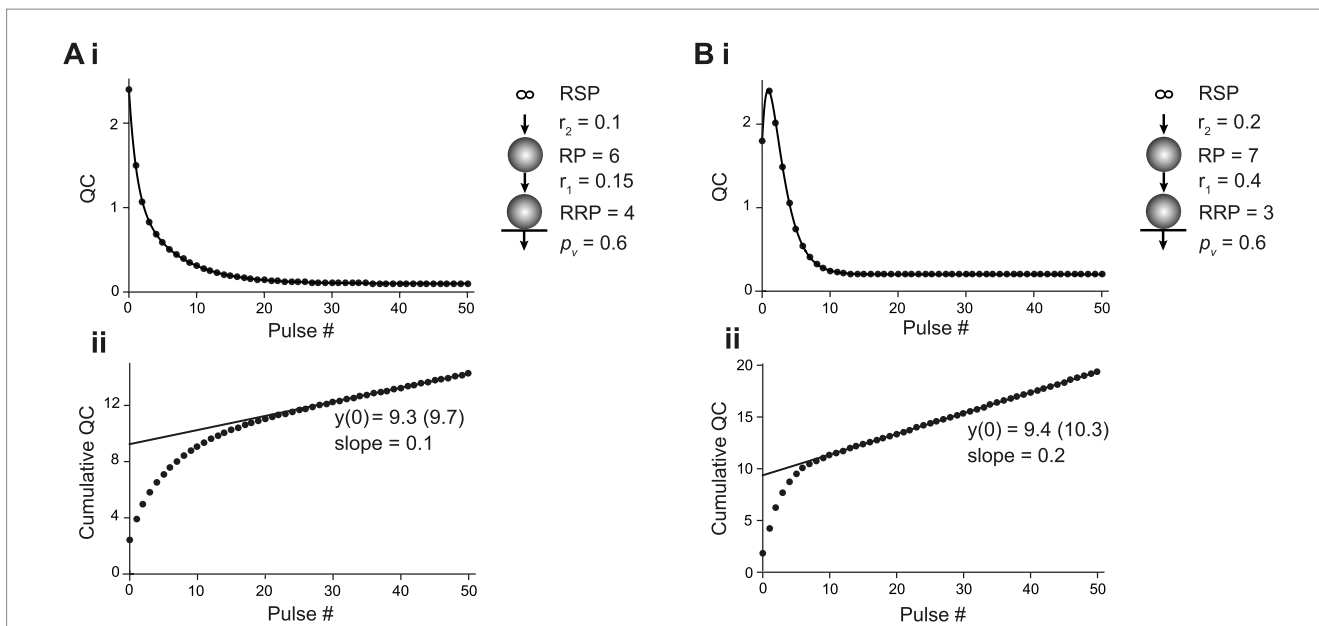
FIGURE 3

CumAna in the SOS model. **(Ai)** SOS model of a depressing synapse. The plot of the quantal content (QC) against pulse number fitted with a double exponential function. The sizes of RRP and RP were 4 and 6, respectively. Replenishment from the infinite RSP to RP occurred with r_2 of 0.1 and the transition of SVs from RP to RRP with r_1 of 0.15. p_v was set to 0.6 throughout the train (scheme to the *right*). **(Aii)** Cumulative quantal content plotted as a function of pulse number. The back-extrapolated line fit to the last 5 data points has a y-intercept at 9.3 (9.7 with correction according to Neher (2015)). Note that this is close to the sum of RP and RRP. Accordingly, dividing the first quantal content by the y-intercept gives a value of 0.26 (0.25) that underestimates p_v. The slope of the line fit is 0.1; i.e., it corresponds to r_2. **(Bi)** As in panel **(Ai)** but for a facilitating synapse. The set values in this simulation were as follows: RRP = 3; RP = 7; r_1 = 0.4; r_2 = 0.2; p_v = 0.6. Note the initial facilitation despite the high p_v, which is due to an increase in the RRP (overfilling). **(Bii)** Cumulative quantal content as a function of pulse number. The line fit has a y-intercept of 9.4 (10.3 following correction) and a slope equal to r_2. Hence, the *y*-intercept is again close to RP plus RRP and the quantity of the first quantal content/y-intercept yields 0.19 (0.17), again underestimating p_v.

0.6 and slower r_1 of 0.1, while RRP2 harbored 7 SVs with lower p_{v2} of 0.3 but faster replenishment with rate constant r_2 of 0.3 (Figure 4). As for the sequential model, the time course of the decrease in quantal content was biexponential (Figure 4A). The line fit in the cumulative quantal content plot had a slope of 0.4, i.e., a value corresponding to the linear sum of r_1 and r_2. The y-intercept had a value close to the total RRP, which means that a larger part of the pool with a low p_v value showed up in the y-intercept (Figure 4B). Consequently, the p_v as reported by dividing the first quantal content by the y-intercept was close to the average between p_{v1} and p_{v2}.

Taken together, these results indicate that biexponential decays in QC or PSC amplitudes during train experiments hint toward the presence of a more complex organization of pools of SVs as proposed in the sequential or the parallel model. However, CumAna alone cannot identify these pools as there is no *a priori* knowledge about the presence of an RP or a subdivision of the RRP. Moreover, the sequential and the parallel model lead to similar results in CumAna. In particular, for the SOS model, the y-intercept reports the sum of RRP and RP (y(0) = RRP + RP), and in the PP model, it reports the sum of the high and low p_v pools (y(0) = RRP$_{\text{high } p}$ + RRP$_{\text{low } p}$).

CumAna in empty sites models

In the next step, we used stochastic simulations to explore the outcome of CumAna if the initial occupancy of the release sites is incomplete (Miki et al., 2016), which we refer to as empty site models. First, we simulated a single RRP model with a fractional release site
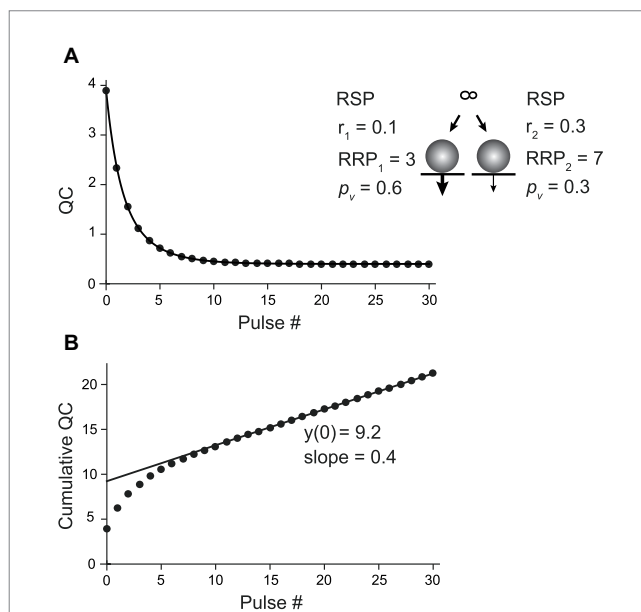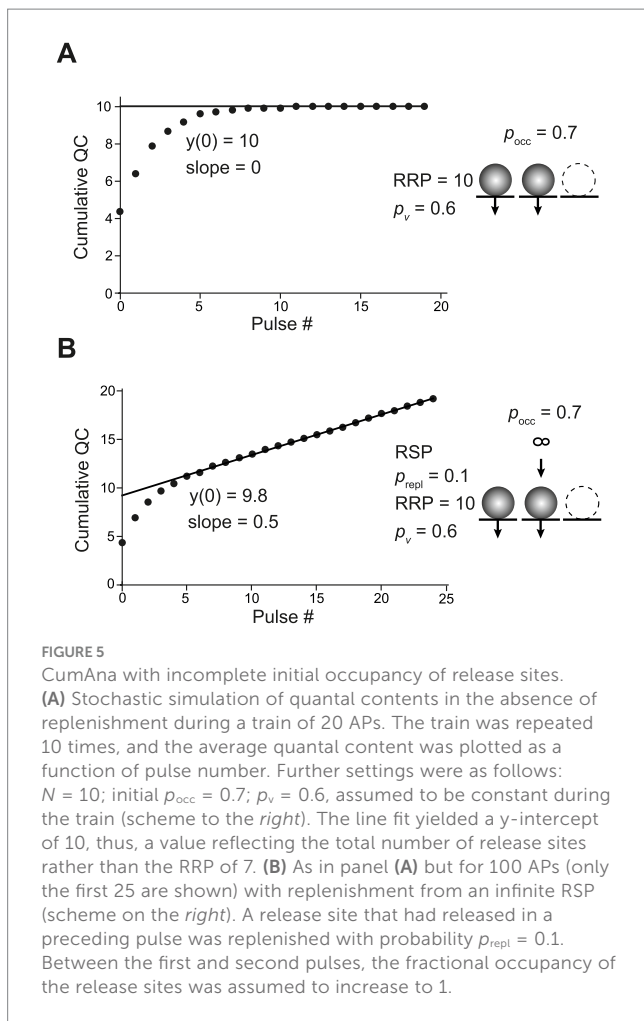

FIGURE 4

CumAna in the PP model. **(A)** Plot of the quantal content (QC) against pulse number fitted with a double exponential function for the PP model of a depressing synapse (scheme in the *inset*). RRP$_1$ and RRP$_2$ harbored 3 and 7 SVs with p_v of 0.6 (thick arrow) and 0.3 (thin arrow), respectively. RRP$_1$ was replenished slower with r_1 = 0.1 and RRP$_2$ faster with r_2 = 0.3. **(B)** Cumulative QC plotted as a function of pulse number (as in Figure 3Aii). The line fit has a y-intercept of 9.2 (9.8 following correction) and a slope of 0.4 (corresponding to r_1 + r_2). The calculated release probability is 0.42 (0.4).

FIGURE 5
CumAna with incomplete initial occupancy of release sites.
(A) Stochastic simulation of quantal contents in the absence of replenishment during a train of 20 APs. The train was repeated 10 times, and the average quantal content was plotted as a function of pulse number. Further settings were as follows: $N = 10$; initial $p_{occ} = 0.7$; $p_v = 0.6$, assumed to be constant during the train (scheme to the *right*). The line fit yielded a y-intercept of 10, thus, a value reflecting the total number of release sites rather than the RRP of 7. **(B)** As in panel **(A)** but for 100 APs (only the first 25 are shown) with replenishment from an infinite RSP (scheme on the *right*). A release site that had released in a preceding pulse was replenished with probability $p_{repl} = 0.1$. Between the first and second pulses, the fractional occupancy of the release sites was assumed to increase to 1.

occupancy of 0.7 in the absence of replenishment (Figure 5A). N was set to 10 with a corresponding RRP of 7 and p_v was set again to 0.6 (Figure 2). Interestingly, the y-intercept of CumAna reported a value of 10 in this scenario. Thus, although the RRP harbored only 7 SVs on average in these simulations, the y-intercept reports the set value for N of 10 (Figure 5A). However, due to the reduced occupancy and the correspondingly smaller RRP the quantal content of the first PSC was only 4.4 rather than 6. Accordingly, the ratio of QC1/y(0) underestimated the true p_v and was only 0.44 instead of 0.6. This value is close to the set value of p_v of 0.6 multiplied by the occupancy of 0.7. Hence, in empty sites models, p_v does not report the intrinsic fusion probability of an SV but rather the fusion probability multiplied by the occupancy (cf. Neher, 2023).

Next, the empty sites simulation was extended by a single replenishment step from the RSP (Figure 5B). In this scenario, the y-intercept reported a value of 9.8, i.e., a value close to but somewhat smaller than the set value for the number of release sites. Accordingly, the ratio of QC1/y(0) again underestimated the true p_v and was 0.43. Depending on the details of the settings for p_v, initial occupancy, and increase in occupancy between pulses, this model could either produce initial facilitation followed by depression or immediate depression (not shown). However, the principle results that the y-intercept reports a value close to the total number of release sites, including those that were empty initially, rather than the RRP was not affected by these differences. Finally, the simulation of empty sites was

extended by the intermediate RP with finite size, resulting in the SES model. As expected from the previous section, the y-intercept currently includes the RP; i.e., in the SES model, y(0) reports the sum of RP, RRP, and empty sites (Table 2). Accordingly, p_v, calculated from QC1 and y(0), will be smaller than the product of fusion probability and release site occupancy.

Taken together, if the initial occupancy of the release sites is incomplete (empty sites models), the y-intercept reports the total N including empty sites rather than the RRP (y(0) $\approx N >$ RRP) and the quantity QC1/y(0) underestimates p_v. In fact, the value of p_v from the CumAna corresponds to the product of the set value of p_v (intrinsic vesicular fusion probability) and occupancy. However, for the SES model, the RP will add to y(0) such that y(0) $\approx N +$ RP and the reported p_v will be smaller than fusion probability times occupancy. It should be noted at this point that RP contributes to y(0) in both sequential models, SOS and SES. We further have to note that there is no *a priori* knowledge of the actual occupancy of the release sites and therefore CumAna alone cannot identify incomplete occupation of release sites. In the following sections, we therefore investigated whether MPFA could be useful to help distinguish increasing release site occupancy as a mechanism of facilitation from a factual increase in the number of release sites.

MPFA with paired pulses in SOS and PP model

As indicated by the above results, CumAna alone cannot distinguish between the different models. Hence, we proceeded by simulating MPFA to see whether a combination of CumAna and MPFA would yield deeper insights. First, we used the SOS model and simulated MPFA with paired pulses at a short interstimulus interval (ISI) and a longer interval between the double pulses that allowed the synapse to return to its initial state, i.e., complete relaxation from any short-term plasticity during the paired pulses with a complete recovery of the RRP to its initial size. We simulated the following two scenarios: first, full initial occupancy of release sites with an actual increase or decrease in the number of N in the second pulse (Figures 6A–C); second, full initial occupancy of release sites with increasing or decreasing p_N in the second pulse, while N stayed constant (Figures 6D–E).

In the first scenario, a parabola fitted to the mean–variance plot of the first PSC amplitudes or quantal contents yielded the nominal value for the number of release sites N as in the above simulations (Figures 2D, 6A). This value of N corresponds to the size of the RRP and excludes the RP. Thus, in comparison with CumAna with the SOS model the N yielded by the first parabola of MPFA is smaller than the y-intercept. The second parabola deviated from the first one in characteristic ways: If N increased between paired pulses, the parabola got wider, whereas it got narrower if N decreased (Figures 6B,C). By contrast, in the second scenario with changes in p_N rather than in N, the points of the second pulses fell to the first parabola. If p_N was increased they were shifted toward higher mean values and if p_N was decreased, they shifted toward smaller means (Figures 6D,E). The results for the second parabolas are consistent with previously published results (Clements and Silver, 2000).

Then, we performed the MPFA with the PP model (Figure 7). A total N of 10 was subdivided into N_1 and N_2. N_1 had a size of 3 with p_{N1}

TABLE 2 Summary of simulation results for SOS, SES, and PP models.

Model	CumAna	MPFA
Sequential RP models		
(i) SOS model (Doussau et al., 2017)	$y(0) = RRP + RP$	1st parabola: $N_1 = N_{occ} = RRP = y_0 - RP$ 2nd parabola: Additional N $N_2 > N_1$ (parabola gets wider)
(ii) SES model (Miki et al., 2016)	$y(0) = RRP + N_{unocc} + RP$	1st parabola: $N_1 = N_{occ} + N_{unocc} = y_0 - RP$ 2nd parabola: Increasing occupancy, fix N $N_2 = N_1$ (second points fall to the first parabola)
=>	$y(0) > N_{1,MPFA}$ $p_v < p_N*$	
Parallel pool model		
PP model (Wölfel et al., 2007)	$y_0 = \sum_i RRP_i$	1st parabola: $N_{MPFA} = \sum_i N_i$
=>	$y(0) = N_{1,MPFA}$ $p_v = p_N*$	

The LS/TS model was not covered in the simulations. With regard to y(0) and N$_{1,MPFA}$ the following results are expected (Neher and Brose, 2018; Neher, 2023): $y(0) = LS + TS + N_{unocc}$ and $N_{1,MPFA} = N_{LS} + N_{TS} + N_{unocc}$, i.e., $y(0) = N_{1,MPFA}$ as in the PP model (see Figure 9). *Average p-values for the same extracellular Ca^{2+} concentration.

set to 0.1, 0.2, 0.4, 0.63, or 0.75 to mimic, e.g., the wash-in of increasing $[Ca^{2+}]_e$. N_2 was set to 7 with p_{N2} set to 0.7 * p_{N1}, representing the pool with lower release probability. In this case, N_{MPFA} reported by the parabolic fit was close to 10; i.e., it reported both the high and the low p_N sites. Thus, for parallel pools, the y-intercept obtained by CumAna and the N_{MPFA} derived by MPFA will be very similar, being identical in theory.

Taken together, these simulations indicate that a combination of CumAna and MPFA can provide a means to distinguish between SOS and PP models. In particular, for SOS the y-intercept will be larger than N estimated by MPFA ($y(0) > N_{MPFA}$), whereas for PP the y-intercept and N will be equal ($y(0) = N_{MPFA}$; Table 2).

MPFA with paired pulses in the empty sites models

We proceeded by analyzing what happens in MPFA if the source of short-term plasticity is a change in the occupancy of release sites, rather than a change in the number of release sites. To analyze the incomplete occupancy of release sites, we started with paired pulses in a presynaptic depletion model, where all N values were initially fully occupied. However, emptied sites were not replenished prior to the second pulse; i.e., the N values were more or less depleted in the second pulse, depending on the quantal content released in the first pulse (Figure 8A). The total N in the simulation remained constant, i.e., merely the occupancy of release sites decreased between the first and second pulses. In this scenario, all points of the second pulse fell to the first parabola albeit at apparently lower p_N values. The shift of the second points was strongest for the highest

nominal p_N settings although the set values for p_N were not changed between pulses; i.e., with regard to the nominal values, p_{N2} was equal to p_{N1}. In fact, the actual values for p_{N2} were equal to the set values for p_N multiplied by the actual occupancy of the N in the second pulse (Figure 8A).

We proceeded by reducing the initial probability of the occupancy (p_{occ1}) of N to 0.7 with a high probability of replenishment (p_{repl}) between pulses of 0.9 (Figure 8Bi) and a total N of 10 (occupied plus unoccupied) that remained constant among pulses as above (SES model). In this SES scenario, the first parabola reported the nominal value of the total N of 10. Notably, also in this scenario the points of the second pulse fell to the first parabola albeit at higher apparent p_N values. For both parabolas, the reported p_N values were given by the nominal p_N values multiplied with the corresponding probabilities of occupancy of the N, i.e., $p_{N1} = p_N * p_{occ1}$ and $p_{N2} = p_N * p_{occ2}$. The occupancy during the second pulse was higher than during the first one due to the high probability of replenishment between pulses, which gave rise to the shift of the second points to apparently higher p_N values. The principle result is that points of the first and the second pulse fall to the same parabola with their location being given by $p_N * p_{occ}$ held for all different initial occupancies and different probabilities of replenishment tested (Figures 8Bii–v). We can therefore conclude that changes in the occupancy of release sites are reminiscent of the changes in p_N simulated in the previous section (Figures 6D,E) and are difficult to distinguish from them.

In summary (Table 2), in an MPFA with paired pulses the parabola will report the total N including those sites that are not occupied by a release-ready SV. The location of the individual points along the parabola will depend on the product of the intrinsic p_N and the probability of occupancy (p_{occ}). Importantly, points of the first and the second pulse fall to the same parabola as long as the total N is constant. On the other hand, if the second parabola is wider than the first one, this is a strong indication of the replenishment of additional release sites. Finally, if the y-intercept from CumAna is larger than N_{MPFA} reported by MPFA this is a strong indication of the presence of a series-connected RP with finite size, whereas in the absence of the RP, the y-intercept will be equal to N_{MPFA}.

Conclusion and discussion

In this paper, we theoretically explored the insights that can be gained into the organization and dynamics of SV pools by combining the experimental methods CumAna and MPFA, including phenomena such as overfilling and the replenishment of new release sites. We used computer simulations to guide our theoretical considerations and focused on two recent sequential vesicle pool models, the SOS (Doussau et al., 2017; Bornschein et al., 2019b) and the SES (Miki et al., 2016). We further covered a traditional PP model that does not harbor a series-connected RP (Wölfel et al., 2007; Mahfooz et al., 2016). In the following, we will summarize our main conclusions and discuss them in a broader context:

(i) The presence of a series-connected RP but also parallel RRPs with SVs differing in their p_v gives rise to a biphasic drop in quantal contents during sustained trains of APs with steady-state depression of synaptic responses. On the other hand, for a single RRP with direct replenishment from the quasi-infinite
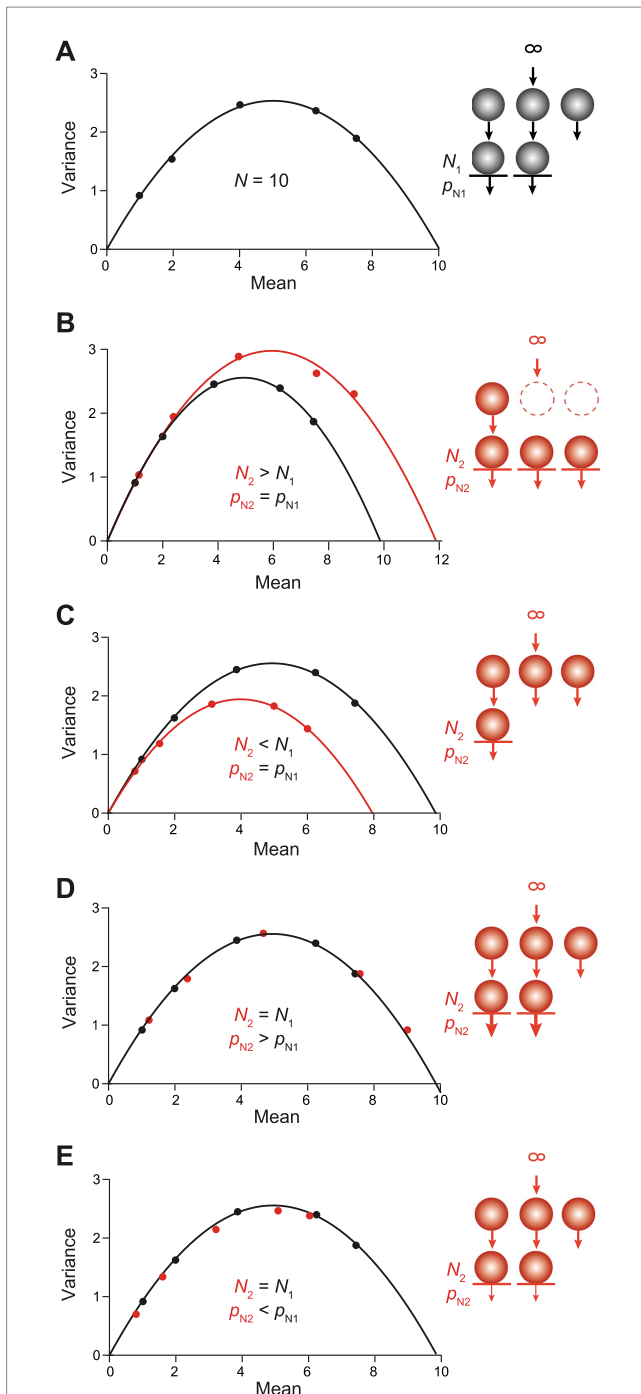
FIGURE 6
MPFA in the SOS model. Sequential models with an RP and short-term plasticity resulting from changes in N or p_N as indicated by the schemes in the *insets* to the right. **(A)** MPFA of the first pulse as described in Figure 2D (p_{N1}: 0.1, 0.2, 0.4, 0.63, 0.75). It is assumed that SVs from the RP do not contribute to the first release process. The parabolic fit yielded an N very close to the set value of 10. **(B)** Black parabola and simulations as in panel **(A)**. The red parabola is the result of N being increased to a value of 12 in the second pulse due to the rapid recruitment of new N from the RP. The p_N values were as in panel **(A)**. **(C)** Same as in panel **(B)** but for N being reduced to 8 in the second pulse due to slow replenishment. **(D)** Black points and parabola as in panel **(A)**. The red points are the result of p_N being increased (thick arrows) in the second pulse (p_{N2}: 0.12, 0.24, 0.48, 0.76, and 0.9), while N was kept constant. Note that the red points fall to the initial black parabola albeit with a rightward shift, i.e., toward higher release probabilities. **(E)** Same as in panel **(D)** but for reduced p_N (thin arrows) in the second pulse (p_{N2}: 0.08, 0.16, 0.32, 0.5, and 0.6).
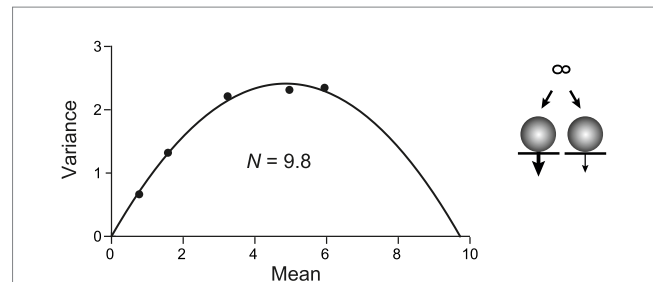
FIGURE 7
MPFA in the PP model. PP model (scheme to the *right*) for two RRPs occupying release sites N_1 (3) and N_2 (7) with p_{N1} (thick arrow) as in Figure 6A and $p_{N2} = 0.7 * p_{N1}$ (thin arrow). MPFA as described in Figure 2D. The parabolic fit yielded N of 9.8, which is close to the set value of $N_1 + N_2$.

RSP, this drop will be monoexponential unless the replenishment rate gets reduced over time. Hence, the biphasic drop can indicate a more complex organization of SV pools but cannot distinguish between sequential and parallel arrangements.

(ii) The y-intercept in CumAna reports the sum of RRP ($=N_{occ}$) plus RP (SOS model: y(0) = RRP + RP) and would also include initially empty release sites (SES model: y(0) = RRP+ N_{unocc} + RP). In the PP model, the y-intercept gives the total RRP (y(0) = $\sum$ RRP$_i$). If the RP were added to the PP model, it would also show up in the y-intercept. The fit of the PP model with RP to experimental data may be superior to that of the SOS or SES models. However, all of these models typically have more parameters and equations than the experimental data can constrain, making them underdetermined already in their current forms.

(iii) The first parabola of MPFA reports the total N, including initially empty sites, but excluding replenishment sites. Hence, we suggest that if y(0) > N_{MPFA} this is a clear indication of the presence of RP vesicles occupying replenishment sites. It should be noted that longer trains of APs are required. Briefer bursts (< 10 APs) may not exhaust the RP and the linear back extrapolation will yield a y-intercept that is closer to the estimate of N from the MPFA but has a strong dependency on the length of the burst. Experimentally, y(0) > N_{MPFA} with long AP trains has been observed at different synapses (see below).

(iv) If the parabola in a paired-pulse experiment gets wider in the second pulse, this results from a factual increase in N (see also Clements and Silver, 2000), whereas a mere increase in the occupancy of N does not change the shape of the parabola. Hence, MPFA with paired pulses provides a means to differentiate a factual increase in N from a mere increase in the occupancy of a fixed number of N as a source of overfilling. Such increase in N has been observed experimentally, for example, at parallel fiber (PF) to Purkinje cell (PC) synapses (Valera et al., 2012; Brachtendorf et al., 2015), but not at PC–PC synapses (Bornschein et al., 2013).

(v) For parallel pools, MPFA reports the total N summed over all sites ($N_{MPFA} = \sum N_i$). Hence, for PP models y(0) will be equal to N_{MPFA}, providing a means to distinguish the PP arrangement from the SOS or SES arrangements.
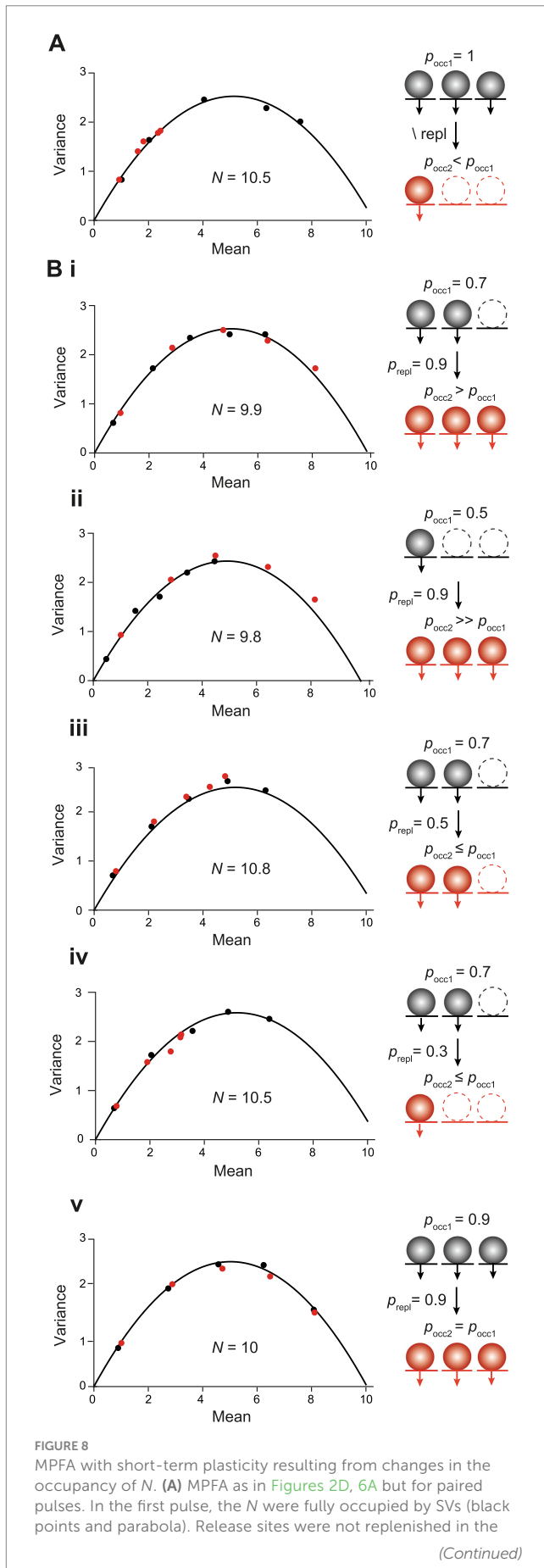
In summary, based on points (ii), (iii), and (v), we suggest that the y-intercept is greater than N_{MPFA} if presynaptic boutons harbor an RP and replenishment sites in series with the RRP ($y(0) > N_{MPFA}$), while both are equal for parallel RRPs without RP ($y_0 = N_{MPFA}$). Biexponential decay of synaptic responses during AP trains thus indicates sequential or parallel pools (i), and the combined use of CumAna and MPFA offers the possibility to distinguish between SOS and SES on the one hand and PP on the other. Finally, MPFA with paired pulses provides a means to identify a factual increase in N as opposed to a mere increase in the occupancy of N; i.e., it provides a means to distinguish between SOS and SES models (Table 2).

The basis of CumAna is the assumption that late during the train the synapse is in a steady state between SVs being released and newly replenished and that the rate of replenishment is constant during the train. Furthermore, for studying changes in pool size, it is important to aim at keeping p_v constant, e.g., by adjusting the $[Ca^{2+}]_e$ in experiments (Neher, 2015). Therefore, in our simulations, we kept both p_v and the replenishment rates constant. p_v was set to 0.6 to meet the additional requirement of depression and no increase in p_v was assumed during the train.

A recent variant of MPFA used trains of APs at 'simple synapses' that harbor only a single active zone, in combination with counting of individual release events by deconvolution (Miki et al., 2016; Miki, 2019). Variance mean analysis was extended there to cover also cumulative values, somewhat reminiscent of a combination of MPFA with CumAna. The quantification of the data relied on more complex modeling and provided evidence for sequential pools with incomplete initial release site occupancy (SES model). The aim of the present study was to probe if the classical and more simple versions of MPFA (Clements and Silver, 2000) and CumAna (Schneggenburger et al., 1999) can provide similarly deep insights into the organization of release sites and vesicle pools in the absence of complex modeling. Our results suggest that a combination of the two methods with canonical parabolic or linear analysis can indeed provide detailed information about the organization of release at the active zone.

The results for the SOS and SES model will not be identical to another recent sequential model in which SVs reversibly shift their state from LS to TS before they can fuse (Neher and Brose, 2018; Neher, 2023). As in the SES model, empty sites occur in the LS/TS
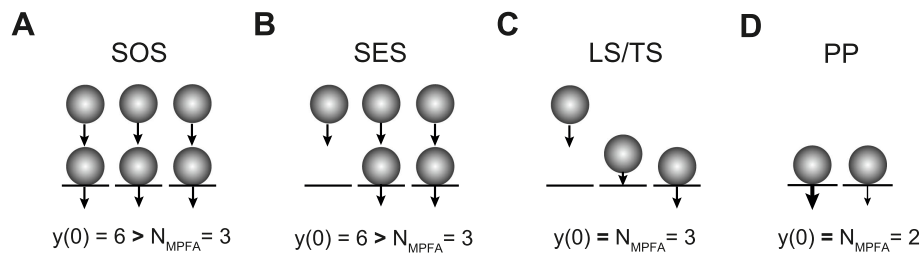
(Continued)

FIGURE 9
Summary of results for sequential and parallel pool models. **(A)** Scheme as in Figure 1. In the SOS model as shown here, the following parameters from CumAna and the first parabola of MPFA would be obtained: y(0) = 6, N_{MPFA} = 3. **(B)** As in **(A)**, but for the SES model: y(0) = 6, N_{MPFA} = 3. **(C)** As in **(A)** but for the LS/TS model: y(0) = 3, N_{MPFA} = 3. **(D)** As in **(A)** but for the PP model: y(0) = 2, N_{MPFA} = 2. Note, that in the SOS and SES model y(0) > N_{MPFA}, while in the LS/TS and PP model y(0) = N_{MPFA} (see Table 2).

model and increasing occupancy of the TS is a major mechanism of facilitation. Similar to the RP in the SOS and SES models, SVs in LS will show up in the y-intercept as the empty sites will do. However, different from vesicles in the RP, LS vesicles will also appear in the N of the MPFA. This means that in the LS/TS model, y(0) and N_{MPFA} could be quite similar, just as in the PP model. Thus, while there are several similarities between the sequential models, there are also crucial differences between the SOS, SES, and LS/TS models. In particular, vesicles of the RP or in LS are not identical (Figure 9). However, the three sequential models need not be mutually exclusive, and, while there is so far no experimental evidence for this, it is well conceivable that at a given synapse more than one type of overfilling mechanism is operational to produce synaptic facilitation.

In our simulations, released quanta were assumed to be perfectly synchronized, which is a simplification compared to real synaptic release as investigated in experiments. In the SOS and SES models, it was further assumed that SVs from the RP do not contribute to the first release. In experiments, CumAna and MPFA are typically based on the analysis of PSC amplitudes. Even with ultra-rapid replenishment (Miki et al., 2016; Doussau et al., 2017) in which SVs from the RP may even contribute to the first PSC, it is more likely that these SVs contribute to the decay of the PSC rather than to its peak amplitude. In addition, in rapid-freezing electron microscopy studies the transient increase in the number of docked SVs was observed only after the stimulation (Kusick et al., 2022). Hence, we think that a non-perfectly synchronized release will not affect the general conclusion of y(0) > N_{MPFA} for the SOS and SES models.

For our theoretical considerations, individual release sites were modeled with linear summation of released quanta and direct "read out" of the number of successes. However, in experiments, the degree of saturation of postsynaptic receptors has to be considered carefully for quantitative estimations of N. In particular, multivesicular release, which appears to be frequent in the brain (Rudolph et al., 2015), may result in receptor saturation and underestimation of N. Fortunately, methods exist to alleviate receptor saturation by the use of competitive antagonists such as γ-DGG at glutamatergic synapses. For a comprehensive discussion of univesicular versus multivesicular release in MPFA, we refer to Silver (2003).

In the PP model also the low p_v pool got fully depleted in our simulations. As the amplitude of the Ca^{2+} signal and the corresponding release rates rapidly drop with increasing distance from the Ca^{2+}

channels (Bucurenciu et al., 2008; Bornschein et al., 2013; Schmidt et al., 2013; Nakamura et al., 2015; Bornschein et al., 2019b; Chen et al., 2024), this may not always be possible to achieve in experiments. In this case, the y-intercept will not report the sum of both RRPs but rather an intermediate value between the size of the high p_v pool and the sum of both pools, i.e., $RRP_{high\,p} < y(0) < RRP_{high\,p} + RRP_{low\,p}$. Then, SVs from $RRP_{low\,p}$ can contribute to the slope of the steady-state phase. In particular, this may arise if p_v is strongly heterogeneous between SVs and/or if SV pools are very large, harboring thousands of SVs such as in the calyx of Held (Neher, 2015). Considering this possibility, the comparison of y-intercept and N_{MPFA} yields y(0) $\leq N_{MPFA}$ for the PP model. However, y(0) > N_{MPFA} as in the SOS and SES models will not occur.

Footprints of our conclusions can be found in experiments on different CNS synapses, including cerebellar, neocortical, or brainstem synapses. At different synapses, changes in the functional presynaptic nanotopography were found during postnatal development. In particular, the coupling distance between voltage-gated Ca^{2+} channels and the synaptic vesicles was found to switch from loose to a tight coupling during development, e.g., at the Calyx of Held (Fedchyshyn and Wang, 2005; Nakamura et al., 2015), PF–PC synapses (Baur et al., 2015) and L5PN–L5PN synapses (Bornschein et al., 2019b). At the latter synapse, evidence was provided that the switch in coupling was accompanied by the maturation of a rapid replenishment pool that transformed the decay time course of EPSC amplitudes during trains of action potentials from mono- to biexponential (Bornschein et al., 2019a).

Cerebellar granule cells (GCs) typically form only a single PF synaptic contact that harbors only a single active zone (Xu-Friedman et al., 2001) with their postsynaptic targets, including PCs and molecular layer interneurons (MLI). These 'simple synapses' are an intensively investigated model for a typical small cortical synapse (Pulido and Marty, 2017; Schmidt, 2019; Silva et al., 2021). MPFA in paired GC–PC recordings quantified N_{MPFA} and p_N to be ~3 and 0.25, respectively (Schmidt et al., 2013). Strikingly, with this very limited immediate resource for transmitter release, PF synapses show long-lasting high-frequency facilitation over up to 30 APs with initially paired-pulse ratios of up to ~3 (Valera et al., 2012; Brachtendorf et al., 2015; Doussau et al., 2017). MPFA with paired pulses at this synapse showed that the parabola in the second pulse got wider than in the first pulse, which was interpreted as a use-dependent factual increase in N as a major source of PPF at these synapses (Valera

et al., 2012; Brachtendorf et al., 2015). Furthermore, the long-lasting high-frequency facilitation of this synapse was explained by a sequential pool model with ultra-rapid, reversible increases in N (Doussau et al., 2017). The current considerations and simulations support this interpretation by ruling out the possibility that an increasing width of the parabola results solely from a mere increase in the occupancy of a fixed number of release sites. However, they do not rule out the possibility that, in addition to the increase in N, there is also incomplete initial occupancy. Incomplete initial occupancy has been detected at MLI–MLI synapses (Trigo et al., 2012) and increasing occupancy of release sites during successive synaptic activations has been suggested at PF–MLI synapses as a mechanism of PPF, using the SES model (Miki et al., 2016). As PF–PC and PF–MLI synapses are formed by the same presynaptic GC, it appears plausible that at PF terminals both mechanisms, increasing N and incomplete initial occupancy, are operational synergistically. For the interesting question of what constitutes an empty release site and more generally how the view of the release site has been changing in recent years, we refer to recent comprehensive reviews (Pulido and Marty, 2017; Neher and Brose, 2018; Silva et al., 2021; Kusick et al., 2022; Neher, 2023).

The prioritization of the sequential over the parallel model was not explicitly justified at PF synapses (but see Doussau et al., 2017). However, the data from CumAna and MPFA show $y(0) > N_{MPFA}$ at PF–PC synapses (Schmidt et al., 2013; Baur et al., 2015), which argues in favor of the sequential model. Similar findings come from an inhibitory cerebellar synapse (Chen et al., 2024) and a neocortical synapse formed between L5PNs (Bornschein et al., 2019a,b). Interestingly, at the latter synapse evidence was found that the RP develops only during synaptic maturation between the first and third postnatal week in mice, thereby changing the short-term plasticity properties (Bornschein et al., 2019a).

Two recent studies explained longer lasting forms of synaptic facilitation, augmentation (Shin et al., 2024), and LTP (Weichard et al., 2023) by overfilling, using sequential pool models. Synaptotagmin 7 (Syt7) was identified earlier as a presynaptic facilitation sensor (Jackman et al., 2016), and it was tempting to speculate that Syt7 might be involved in driving overfilling (Bornschein and Schmidt, 2019). Indeed, Shin et al. (2024) currently provided evidence that Syt7 drives overfilling.

The PP model was used to simulate the biphasic time course of release at another important model synapse, the calyx of Held (Wölfel et al., 2007). However, a biphasic time course of release can also arise from sequential pools of SVs [see point (i)] and it has recently been shown that the LS/TS model describes release and short-term plasticity at the calyx very well (Lin et al., 2022).

Results on differences in short-term plasticity and also presynaptic forms of LTP are frequently considered to reflect differences in p_v. The sequential pool models suggest an alternative interpretation (Neher, 2023). The dynamics of reversible vesicle priming, varying occupancy of release sites, and the replenishment of new release sites make major contributions to short-term plasticity. The simple theoretical framework proposed here provides a means to identify signatures of the RP without the need for complex computer simulations. It is based on the combination of two standard physiological methods, cumulative analysis of PSC amplitudes, and multiple probability fluctuation analysis.

Data availability statement

Author contributions

GB: Visualization, Writing – original draft, Writing – review & editing. SB: Visualization, Writing – original draft, Writing – review & editing. HS: Conceptualization, Funding acquisition, Investigation, Methodology, Writing – original draft, Writing – review & editing.

Funding

Acknowledgments

Conflict of interest

The authors declare that the research was conducted in the absence of any commercial or financial relationships that could be construed as a potential conflict of interest.

The author(s) declared that they were an editorial board member of Frontiers, at the time of submission. This had no impact on the peer review process and the final decision.

Generative AI statement

The authors declare that no Gen AI was used in the creation of this manuscript.

Publisher's note

References

Aldahabi, M., Neher, E., and Nusser, Z. (2024). Different states of synaptic vesicle priming explain target cell type–dependent differences in neurotransmitter release. *Proc. Natl. Acad. Sci.* 121:e2322550121. doi: 10.1073/pnas.2322550121

Baur, D., Bornschein, G., Althof, D., Watanabe, M., Kulik, A., Eilers, J., et al. (2015). Developmental tightening of cerebellar cortical synaptic influx-release coupling. *J. Neurosci.* 35, 1858–1871. doi: 10.1523/JNEUROSCI.2900-14.2015

Bornschein, G., Arendt, O., Hallermann, S., Brachtendorf, S., Eilers, J., and Schmidt, H. (2013). Paired-pulse facilitation at recurrent Purkinje neuron synapses is independent of calbindin and parvalbumin during high-frequency activation. *J. Physiol.* 591, 3355–3370. doi: 10.1113/jphysiol.2013.254128

Bornschein, G., Brachtendorf, S., and Schmidt, H. (2019a). Developmental increase of neocortical presynaptic efficacy via maturation of vesicle replenishment. *Front. Synaptic. Neurosci.* 11:36. doi: 10.3389/fnsyn.2019.00036

Bornschein, G., Eilers, J., and Schmidt, H. (2019b). Neocortical high probability release sites are formed by distinct Ca^{2+} channel-to-release sensor topographies during development. *Cell Rep.* 28:e1414, 1410–1418.e4. doi: 10.1016/j.celrep.2019.07.008

Bornschein, G., and Schmidt, H. (2019). Synaptotagmin Ca^{2+} sensors and their spatial coupling to presynaptic Ca_v channels in central cortical synapses. *Front. Mol. Neurosci.* 11:494. doi: 10.3389/fnmol.2018.00494

Brachtendorf, S., Eilers, J., and Schmidt, H. (2015). A use-dependent increase in release sites drives facilitation at calretinin-deficient cerebellar parallel-fiber synapses. *Front. Cell. Neurosci.* 9:27. doi: 10.3389/fncel.2015.00027

Bucurenciu, I., Kulik, A., Schwaller, B., Frotscher, M., and Jonas, P. (2008). Nanodomain coupling between Ca^{2+} channels and Ca^{2+} sensors promotes fast and efficient transmitter release at a cortical GABAergic synapse. *Neuron* 57, 536–545. doi: 10.1016/j.neuron.2007.12.026

Chen, J. J., Kaufmann, W. A., Chen, C., Arai, I., Kim, O., Shigemoto, R., et al. (2024). Developmental transformation of Ca^{2+} channel-vesicle nanotopography at a central GABAergic synapse. *Neuron* 112, 755–771.e9. doi: 10.1016/j.neuron.2023.12.002

Clements, J. D., and Silver, R. A. (2000). Unveiling synaptic plasticity: a new graphical and analytical approach. *Trends Neurosci.* 23, 105–113. doi: 10.1016/S0166-2236(99)01520-9

Del Castillo, J., and Katz, B. (1954). Quantal components of the end-plate potential. *J. Physiol.* 124, 560–573. doi: 10.1113/jphysiol.1954.sp005129

Doussau, F., Schmidt, H., Dorgans, K., Valera, A. M., Poulain, B., and Isope, P. (2017). Frequency-dependent mobilization of heterogeneous pools of synaptic vesicles shapes presynaptic plasticity. *eLife* 6:e28935. doi: 10.7554/eLife.28935

Eshra, A., Schmidt, H., Eilers, J., and Hallermann, S. (2021). Calcium dependence of neurotransmitter release at a high fidelity synapse. *eLife* 10:e70408. doi: 10.7554/eLife.70408

Fatt, P., and Katz, B. (1952). Spontaneous subthreshold activity at motor nerve endings. *J. Physiol.* 117, 109–128. doi: 10.1113/jphysiol.1952.sp004735

Fedchyshyn, M. J., and Wang, L. Y. (2005). Developmental transformation of the release modality at the calyx of held synapse. *J. Neurosci.* 25, 4131–4140. doi: 10.1523/JNEUROSCI.0350-05.2005

Hallermann, S., Fejtova, A., Schmidt, H., Weyhersmüller, A., Silver, R. A., Gundelfinger, E. D., et al. (2010). Bassoon speeds vesicle reloading at a central excitatory synapse. *Neuron* 68, 710–723. doi: 10.1016/j.neuron.2010.10.026

Heuser, J. E., Reese, T. S., Dennis, M. J., Jan, Y., Jan, L., and Evans, L. (1979). Synaptic vesicle exocytosis captured by quick freezing and correlated with quantal transmitter release. *J. Cell Biol.* 81, 275–300. doi: 10.1083/jcb.81.2.275

Jackman, S. L., Turecek, J., Belinsky, J. E., and Regehr, W. G. (2016). The calcium sensor synaptotagmin 7 is required for synaptic facilitation. *Nature* 529, 88–91. doi: 10.1038/nature16507

Kusick, G. F., Chin, M., Raychaudhuri, S., Lippmann, K., Adula, K. P., Hujber, E. J., et al. (2020). Synaptic vesicles transiently dock to refill release sites. *Nat. Neurosci.* 23, 1329–1338. doi: 10.1038/s41593-020-00716-1

Kusick, G. F., Ogunmowo, T. H., and Watanabe, S. (2022). Transient docking of synaptic vesicles: implications and mechanisms. *Curr. Opin. Neurobiol.* 74:102535. doi: 10.1016/j.conb.2022.102535

Lin, K.-H., Taschenberger, H., and Neher, E. (2022). A sequential two-step priming scheme reproduces diversity in synaptic strength and short-term plasticity. *Proc. Natl. Acad. Sci.* 119:e2207987119. doi: 10.1073/pnas.2207987119

Mahfooz, K., Singh, M., Renden, R., and Wesseling, J. F. (2016). A well-defined readily releasable Pool with fixed capacity for storing vesicles at Calyx of held. *PLoS Comput. Biol.* 12:e1004855. doi: 10.1371/journal.pcbi.1004855

Malagon, G., Miki, T., Llano, I., Neher, E., and Marty, A. (2016). Counting vesicular release events reveals binomial release statistics at single glutamatergic synapses. *J. Neurosci.* 36, 4010–4025. doi: 10.1523/JNEUROSCI.4352-15.2016

Meyer, A. C., Neher, E., and Schneggenburger, R. (2001). Estimation of quantal size and number of functional active zones at the calyx of held synapse by nonstationary EPSC variance analysis. *J. Neurosci.* 21, 7889–7900. doi: 10.1523/JNEUROSCI.21-20-07889.2001

Miki, T. (2019). What we can learn from cumulative numbers of vesicular release events. *Front. Cell. Neurosci.* 13:257. doi: 10.3389/fncel.2019.00257

Miki, T., Malagon, G., Pulido, C., Llano, I., Neher, E., and Marty, A. (2016). Actin- and myosin-dependent vesicle loading of presynaptic docking sites prior to exocytosis. *Neuron* 91, 808–823. doi: 10.1016/j.neuron.2016.07.033

Nakamura, Y., Harada, H., Kamasawa, N., Matsui, K., Rothman, J. S., Shigemoto, R., et al. (2015). Nanoscale distribution of presynaptic Ca^{2+} channels and its impact on vesicular release during development. *Neuron* 85, 145–158. doi: 10.1016/j.neuron.2014.11.019

Neher, E. (2015). Merits and limitations of vesicle pool models in view of heterogeneous populations of synaptic vesicles. *Neuron* 87, 1131–1142. doi: 10.1016/j.neuron.2015.08.038

Neher, E. (2023). Interpretation of presynaptic phenotypes of synaptic plasticity in terms of a two-step priming process. *J. Gen. Physiol.* 156:e202313454. doi: 10.1085/jgp.202313454

Neher, E., and Brose, N. (2018). Dynamically primed synaptic vesicle states: key to understand synaptic short-term plasticity. *Neuron* 100, 1283–1291. doi: 10.1016/j.neuron.2018.11.024

Pulido, C., and Marty, A. (2017). Quantal fluctuations in central mammalian synapses: functional role of vesicular docking sites. *Physiol. Rev.* 97, 1403–1430. doi: 10.1152/physrev.00032.2016

Rudolph, S., Tsai, M. C., Von Gersdorff, H., and Wadiche, J. I. (2015). The ubiquitous nature of multivesicular release. *Trends Neurosci.* 38, 428–438. doi: 10.1016/j.tins.2015.05.008

Schmidt, H. (2019). Control of presynaptic parallel fiber efficacy by activity-dependent regulation of the number of occupied release sites. *Front. Syst. Neurosci.* 13:30. doi: 10.3389/fnsys.2019.00030

Schmidt, H., Brachtendorf, S., Arendt, O., Hallermann, S., Ishiyama, S., Bornschein, G., et al. (2013). Nanodomain coupling at an excitatory cortical synapse. *Curr. Biol.* 23, 244–249. doi: 10.1016/j.cub.2012.12.007

Schneggenburger, R., Meyer, A. C., and Neher, E. (1999). Released fraction and total size of a pool of immediately available transmitter quanta at a calyx synapse. *Neuron* 23, 399–409. doi: 10.1016/S0896-6273(00)80789-8

Shin, J., Lee, S. Y., Kim, Y., and Lee, S.-H. (2024). Progressive overfilling of readily releasable pool underlies short-term facilitation at recurrent excitatory synapses in layer 2/3 of the rat prefrontal cortex. *eLife*. doi: 10.7554/elife.102923.1

Silva, M., Tran, V., and Marty, A. (2021). Calcium-dependent docking of synaptic vesicles. *Trends Neurosci.* 44, 579–592. doi: 10.1016/j.tins.2021.04.003

Silva, M., Tran, V., and Marty, A. (2024). A maximum of two readily releasable vesicles per docking site at a cerebellar single active zone synapse. *eLife* 12:RP91087. doi: 10.7554/eLife.91087

Silver, R. A. (2003). Estimation of nonuniform quantal parameters with multiple-probability fluctuation analysis: theory, application and limitations. *J. Neurosci. Methods* 130, 127–141. doi: 10.1016/j.jneumeth.2003.09.030

Thanawala, M. S., and Regehr, W. G. (2013). Presynaptic calcium influx controls neurotransmitter release in part by regulating the effective size of the readily releasable Pool. *J. Neurosci.* 33, 4625–4633. doi: 10.1523/jneurosci.4031-12.2013

Trigo, F. F., Sakaba, T., Ogden, D., and Marty, A. (2012). Readily releasable pool of synaptic vesicles measured at single synaptic contacts. *Proc. Natl. Acad. Sci.* 109, 18138–18143. doi: 10.1073/pnas.1209798109

Valera, A. M., Doussau, F., Poulain, B., Barbour, B., and Isope, P. (2012). Adaptation of granule cell to Purkinje cell synapses to high-frequency transmission. *J. Neurosci.* 32, 3267–3280. doi: 10.1523/jneurosci.3175-11.2012

Weichard, I., Taschenberger, H., Gsell, F., Bornschein, G., Ritzau-Jost, A., Schmidt, H., et al. (2023). Fully-primed slowly-recovering vesicles mediate presynaptic LTP at neocortical neurons. *Proc. Natl. Acad. Sci. USA* 120:e2305460120. doi: 10.1073/pnas.2305460120

Wender, M., Bornschein, G., Brachtendorf, S., Hallermann, S., Eilers, J., and Schmidt, H. (2023). $Ca_v2.2$ channels sustain vesicle recruitment at a mature glutamatergic synapse. *J. Neurosci.* 43, 4005–4018. doi: 10.1523/jneurosci.1279-22.2023

Wölfel, M., Lou, X., and Schneggenburger, R. (2007). A mechanism intrinsic to the vesicle fusion machinery determines fast and slow transmitter release at a large CNS synapse. *J. Neurosci.* 27, 3198–3210. doi: 10.1523/JNEUROSCI.4471-06.2007

Xu-Friedman, M. A., Harris, K. M., and Regehr, W. G. (2001). Three-dimensional comparison of ultrastructural characteristics at depressing and facilitating synapses onto cerebellar Purkinje cells. *J. Neurosci.* 21, 6666–6672. doi: 10.1523/JNEUROSCI.21-17-06666.2001

Glossary

SV - Synaptic vesicle

PSC - Postsynaptic current amplitude; PSC = $p\,N\,q$

QC - Quantal content quantifying the amount of release from the presynaptic terminal; QC = $p\,N$

CumAna - Cumulative analysis, i.e., analysis of cumulative QCs or PSCs; a method for estimating the size of the RRP and the vesicular release probability

y(0) - y-intercept of CumAna used to estimate the size of the RRP

MPFA - Multiple probability fluctuation analysis; a method to estimate the quantal synaptic parameters

P - Release probability in general

p_v - p per vesicle:

p_v = PSC1/RRP or QC1/RRP

Calculated from CumAna as

p_v = PSC1/y(0) or QC1/y(0)

p_N - p per release site; reported by MPFA

p_{occ} - Probability that a given release site is occupied

p_{repl} - Probability that an emptied release site gets replenished between two pulses

N - Number of release sites including occupied and non-occupied sites

N_{occ} - Release sites occupied by a release-ready vesicle

N_{unocc} - Unoccupied release sites, empty release sites

N_{MPFA} - Binominal parameter for N reported by MPFA

q - Quantal size: The postsynaptic response elicited by the release of a single vesicle

F - Synaptic failure rate summed over all release sites forming the total synaptic connection:

$F = (1 - p_N)^N$

$F = (1 - p_v)^{RRP}$

S - Synaptic success rate:

S = 1 - F

r - Rate constant of replenishment

LS - Loosely tethered state of a vesicle

TS - Tightly tethered state of a vesicle; SVs in TS form the RRP in the narrower sense

RRP - Ready releasable pool of vesicles; equivalent to SVs in TS

RP - Exhaustible rapid replenishment pool formed by SVs that occupy replenishment sites; Ultra rapid transition from RP to RRP can cause overfilling. RP-RRP-transition is reversible on a slower timescale. Not identical to LS.

RSP, ∞ - Infinite reserve pool

overfilling - General term for a reversible increase in the RRP or the number of release sites or their occupancy